J. of Electromagn. Waves and Appl., Vol. 18, No. 7, 879–897, 2004

ESTIMATING ACCURACY OF MOM SOLUTIONS ON ARBITRARY TRIANGULATED 3-D GEOMETRIES BASED ON EXAMINATION OF BOUNDARY CONDITIONS PERFORMANCE AND ACCURATE DERIVATION OF SCATTERED FIELDS

F. G. Bogdanov and R. G. Jobava

EMCoS, EM Consulting and Software, Ltd.
8 Ingorokva Str., 0108 Tbilisi, Georgia

S. Frei

EMC Center, AUDI AG
Ingolstadt, Germany

Abstract—A new error metric is applied for estimating accuracy of MoM solutions on purely 3-D geometries using triangle doublet basis functions. This error metric is based on checking boundary conditions performance (BCP) on scatterer surface and shown to be suited for arbitrary 3-D geometries including open ones. First, accurate expressions for the scattered field are derived to be valid at any observation points including those on the surface of triangles. Further, BCP error metric is examined for estimating accuracy of the scattering problem solution on open cube geometry, and to find the correlation of BCP error with that for near-field characteristics. Finally, BCP error metric is applied to estimate accuracy of MoM solutions on realistic car model, and to find the contributions of its elements to the total error.

1. INTRODUCTION

The Method of Moments (MoM) [1] is nowadays widely used for solving EM and EMC problems on complicated surface and wire configurations [2–4] including those encountered in automotive industry [5]. The practical value of the obtained solutions and of predictions done depends in large extent on the attained solution accuracy. However, although much effort was done [6–10] (this list is by no means complete), a convenient method for estimating accuracy of MoM solutions on arbitrary geometries is lacking till now.

The experimental validation of numerical solutions for the complicated geometries appears to be a difficult, lengthy, expensive, and practically unrepeatable procedure [6]. Besides, measurements themselves are regarded as models involving additional inaccuracy [7]. Further, comparison of MoM solutions with accurate (benchmark) solutions [8] may be practically done only for the selected (benchmark) geometries, that makes this method inefficient for arbitrary geometries. That is why, in spite of existing mathematical basis [9], estimating accuracy of MoM solutions is frequently done by convergence analyzing [10], i.e., comparison of the obtained solution with those calculated for the refined meshing of geometry. However, this method usually requires computational costs exceeding those for the obtained solution in scores of times. Due to this reason, the development of the convenient method to estimate accuracy of MoM solutions on arbitrary geometries is still required.

A natural criterion to estimate accuracy of MoM solutions is the examination of boundary conditions performance (BCP) on scatterer surface [11, 12]. However, difficulties arise when applying this criterion for arbitrary geometries. First, existing error metric for comparing fields fails when considering open geometries including plates and other geometries with free edges. Further, evaluation of BCP error needs calculation of scattered field on the scatterer surface, that cannot be directly done by most of existing MoM codes, in which the observation points on triangle plane are considered as singular [13]. Moreover, difficulties arise when normalizing BCP error to properly characterize the total error on the structure.

This work overcomes the difficulties above, suggesting the proper BCP error metric to be suited to arbitrary 3-D geometries including that for a realistic car. First, the proper BCP error metric is introduced, and accurate expressions of scattered fields for triangle-doublet basis functions [14] are derived to be valid at any observation points including those on the triangle plane. Then, BCP error metric is applied to estimate the scattering problem solution accuracy on open cube geometry. A close correlation of BCP error with those for current and charge distributions is revealed based on rather accurate solution for the sufficiently fine cube geometry. Finally, BCP error metric is applied to estimate accuracy of MoM solutions on the realistic car geometry, and to find the contributions of its elements to the total error on the structure. All the calculations were performed using original MoM-based code, which utilizes new solutions for the potential integrals [15].

This work is organized as follows. Section 2 introduces BCP error metric and derives the accurate expressions for the scattered fields. Section 3 examines the total and partial BCP errors on open cube and realistic car model geometries. Section 4 discusses the presented results and merits of the BCP error metric. Finally, Section 6 outlines our conclusions.

2. METHOD

2.1. Error Metric

The convergence of MoM solutions is traditionally verified by comparing the obtained results with those calculated for the refined geometries. In this way, accuracy of these solutions may be treated as [8]

$$\varepsilon_J[\%]100\frac{\int\limits_S \left|\vec{J}_S - \vec{J}_{S0}\right| dS}{\int\limits_S \left|\vec{J}_{S0}\right| dS} \tag{1}$$

where $\vec{J}_S$ and $\vec{J}_{S0}$ are, respectively, approximate and accurate (benchmark) solutions for the surface currents, and integration is performed over the scatterer surface S. The error metric (1) presents the relative error of mean absolute value (MAV) of current deviation on the boundary surface. As shown in [8], only this error metric is valid, due to the edge effect, for estimating accuracy of the surface currents on arbitrary surfaces including open ones.

The drawback of error estimation (1) is that it needs either inspection of the convergence of solutions for a number of geometries, or knowledge of accurate (benchmark) solutions for the geometry analyzed. However, the latter may be practically done only for selected (benchmark) geometries. To estimate accuracy of MoM solutions for arbitrary geometries of interest, it is natural to examine boundary conditions performance (BCP) on the scatterer surface [11, 12]. In this way, we intend to define a suitable error metric, which is dependent, in turn, on the kind of integral equations to be used in MoM calculations.

For closed surfaces, BCP error metric could be established based on the root-mean square (RMS) value of the correspondent component of the total field normalized to that for the incident field as

$$\varepsilon_{E,RMS}[\%] = 100\frac{\sqrt{\int\limits_S \left|\vec{n}\times(\vec{E}^{sc}+\vec{E}^{inc})\right|^2 dS}}{\sqrt{\int\limits_S \left|\vec{n}\times\vec{E}^{inc}\right|^2 dS}} \tag{2a}$$

for electric field integral equations (EFIE) and

$$\varepsilon_{H,RMS}[\%] = 100\frac{\sqrt{\int\limits_S \left|\vec{n}\times(\vec{H}^{sc}+\vec{H}^{inc})\right|^2 dS}}{\sqrt{\int\limits_S \left|\vec{n}\times\vec{H}^{inc}\right|^2 dS}} \tag{2b}$$

for magnetic field integral equations (MFIE). Here $\vec{E}^{sc}$, $\vec{H}^{sc}$ and $\vec{E}^{inc}$, $\vec{H}^{inc}$ are the scattered and incident fields, respectively, S is the scatterer surface, and $\vec{n}$ is the normal to this surface.

However, RMS error metrics (2) cannot be applied to open structures due to the edge effect, since numerators in formulas (2) become unbounded because of the fields singularity in the vicinity of free edges. Indeed, the scattered field components normal to the edge tends to infinity as reciprocal of the root of the distance from this edge [16]. Therefore, the integrals in numerators of (2) diverge for open structures including free edges.

To define the BCP error metric valid for arbitrary structures, including open ones, we overcome the convergence problems above introducing, similar to (1), MAV error metrics, instead of RMS error metrics of (2), as

$$\varepsilon_E[\%] = 100\frac{\int\limits_S \left|\vec{n}\times(\vec{E}^{sc}+\vec{E}^{inc})\right| dS}{\int\limits_S \left|\vec{n}\times\vec{E}^{inc}\right| dS} \tag{3a}$$

$$\varepsilon_H[\%] = 100\frac{\int\limits_S \left|\vec{n} \times (\vec{H}^{sc} + \vec{H}^{inc})\right| dS}{\int\limits_S \left|\vec{n} \times \vec{H}^{inc}\right| dS} \tag{3b}$$

to be used for EFIE and MFIE, respectively. Emphasize, that BCP error metrics (3) directly indicate how well the obtained solution satisfies the formulated problem. Since numerators in formulas (3) are bounded for any geometries, including open ones, these error metrics are suited for considering arbitrary 3-D geometries, including those encountered in automotive industry.

The estimation of (3) needs calculation of the scattered fields directly on the scatterer surface. However, this point was paid less attention in MoM literature for triangulated geometries, and observation points on the scatterer surface are considered to be singular as in [13]. For this purpose, we derive below the accurate expressions for the scattered fields being bounded at any observation points including those on the surface of triangles.

2.2. Accurate Derivation of the Scattered Field

As is well known, the scattered field at any point of space may be defined as

$$\vec{E}^{sc} = -i\omega\vec{A} - \vec{\nabla}\Phi, \qquad \vec{H}^{sc} = \frac{1}{\mu}\vec{\nabla} \times \vec{A}, \tag{4}$$

where potentials $\vec{A}$ and Φ are expressed via the currents $\vec{J}$ on the scatterer surface S as

$$\vec{A}(\vec{r}\,) = \frac{\mu}{4\pi}\int\limits_S \vec{J}\,\frac{e^{-ikR}}{R}dS, \tag{5}$$

$$\Phi(\vec{r}\,) = -\frac{1}{4\pi i\omega\varepsilon}\int\limits_S \vec{\nabla}'_S \cdot \vec{J}\,\frac{e^{-jkR}}{R}dS \tag{6}$$

where ε and μ are, respectively, permittivity and permeability of surrounding medium, k is a wavenumber, ω is a cycle frequency of excitation, $R = |\vec{r} - \vec{r}\,'|$ is the distance between the observation point $\vec{r}$ and source point $\vec{r}\,'$, and time dependence is assumed as $\exp(i\omega t)$.

In MoM calculations, the current $\vec{J}$ is represented in terms of the known basis functions $\vec{f}_n$ as

$$\vec{J}(\vec{r}\,') = \sum_{n=1}^{N} I_n \vec{f}_n(\vec{r}\,') \tag{7}$$

Once the MoM solution for unknown coefficients I_n is obtained, and surface current $\vec{J}$ is known, formulas (4)–(6) describe, in principle, scattered field at any observation point. However, in case of triangulated structure, these fields are usually expressed through the potential integrals, each of which becomes singular on the triangle plane. For this reason, these points are falsely considered as singular in most of the existing MoM codes.

Below, we will obtain bounded expressions for the scattered fields at any observation points for the well-known sub-domain triangle doublet basis functions [14]

$$\vec{f}_n(\vec{r}\,') = \begin{cases} \dfrac{l_n}{2A_n^+}\vec{\rho}_n^{\,+} & \vec{r}\,' \text{ in } T_n^+ \\ \dfrac{l_n}{2A_n^-}\vec{\rho}_n^{\,-} & \vec{r}\,' \text{ in } T_n^- \end{cases} \tag{8}$$

defined on a pair of the adjacent triangles $T_n^{\pm}$ with areas $A_n^{\pm}$ and a common edge of the length l_n. Here, the vectors $\vec{\rho}_n^{\,\pm} = \pm(\vec{r}\,' - \vec{r}_n^{\,\pm})$ are the local position vectors of the source point $\vec{r}\,'$ on the triangle plane, $\vec{r}_n^{\,\pm}$ are the position vectors of the remote vertices, and sign (+ or −) in sub-indexes indicates whether the positive current reference direction is out of or into the triangle.

To determine the scattered fields (4) for the current representation (7) and basis functions (8), it is necessary to find the contributions to these fields of the pairs of partial potentials $\vec{A}_n^{\pm}, \vec{\nabla}\Phi_n^{\pm}$ and $\vec{\nabla} \times \vec{A}_n^{\pm}$, associated with n-th basis function (8).

For this purpose, let us first, following [14], introduce within triangles $T_n^{\pm}$ the normalised area coordinates [17] of the source point $\vec{r}$: $\zeta = A_1/A_n^{\pm}$, $\xi = A_2/A_n^{\pm}$, and $\eta = A_3/A_n^{\pm}$, where A_i are the areas of subtriangles with remote vertices $\vec{r}_i$, and $A_1 + A_2 + A_3 = A_n^{\pm}$. Then, position vector $\vec{r}\,'$ of the source point on triangle $T_n^{\pm}$ may be represented in area coordinates as [14]

$$\vec{r}\,' = \zeta r_1 + \xi r_3 + \eta r_3 \tag{9}$$

Further, we use vector identities [18]

$$\vec{\nabla} \times \left[\frac{e^{-ikR}}{R}\vec{f}_n(\vec{r}\,')\right] = \vec{\nabla}\frac{e^{-ikR}}{R} \times \vec{f}_n(\vec{r}\,')$$

$$\vec{\nabla}\frac{e^{-ikR}}{R} = \left(-ik - \frac{1}{R}\right)\frac{\vec{R}}{R}\frac{e^{-ikR}}{R}$$

to obtain the following expressions for the unknown partial potentials

$$\vec{A}_n^{\pm} = \pm\frac{\mu\ell_n}{4\pi}\left[\left(\vec{r}_1 - \vec{r}_n^{\,\pm}\right)I_0 + \left(\vec{r}_2 - \vec{r}_1\right)I_\xi + \left(\vec{r}_3 - \vec{r}_1\right)I_\eta\right] \tag{10}$$

$$\vec{\nabla}\Phi_n^{\pm} = \mp\frac{\ell_n}{i2\pi\omega\varepsilon}\left[(\vec{r}-\vec{r}_1)\,\tilde{I}_0 - (\vec{r}_2-\vec{r}_1)\,\tilde{I}_\xi - (\vec{r}_3-\vec{r}_1)\,\tilde{I}_\eta\right] \quad (11)$$

$$\begin{aligned}\vec{\nabla}\times\vec{A}_n^{\pm} &= \pm\frac{\mu\ell_n}{4\pi}\Big\{(\vec{r}-\vec{r}_1)\times(\vec{r}_1-\vec{r}_n^{\,\pm})\tilde{I}_0 + (\vec{r}-\vec{r}_n^{\,\pm}) \\ &\quad \times\left[(\vec{r}_2-\vec{r}_1)\tilde{I}_\xi + (\vec{r}_3-\vec{r}_1)\tilde{I}_\eta\right]\Big\} \qquad (12)\end{aligned}$$

where

$$I_0 = \int_{\eta=0}^{1}\int_{\xi=0}^{1-\eta}\left(\frac{e^{-ikR}-1}{R}\right)d\xi d\eta + I_0' \quad (13)$$

$$I_\xi = \int_{\eta=0}^{1}\int_{\xi=0}^{1-\eta}\xi\left(\frac{e^{-ikR}-1}{R}\right)d\xi d\eta + I_\xi' \quad (14)$$

$$I_\eta = \int_{\eta=0}^{1}\int_{\xi=0}^{1-\eta}\eta\left(\frac{e^{-ikR}-1}{R}\right)d\xi d\eta + I_\eta' \quad (15)$$

and

$$\tilde{I}_0 = \int_{\eta=0}^{1}\int_{\xi=0}^{1-\mu}\left[\left(-ik-\frac{1}{R}\right)\frac{e^{-ikR}}{R^2}+\frac{k^2}{2R}+\frac{1}{R^3}\right]d\xi d\eta - \frac{k^2}{2}I_0' - I_0'' \quad (16)$$

$$\tilde{I}_\xi = \int_{\eta=0}^{1}\int_{\xi=0}^{1-\mu}\left[\left(-ik-\frac{1}{R}\right)\frac{e^{-ikR}}{R^2}+\frac{k^2}{2R}+\frac{1}{R^3}\right]\xi d\xi d\eta - \frac{k^2}{2}I_\xi' - I_\xi'' \quad (17)$$

$$\tilde{I}_\eta = \int_{\eta=0}^{1}\int_{\xi=0}^{1-\mu}\left[\left(-ik-\frac{1}{R}\right)\frac{e^{-ikR}}{R^2}+\frac{k^2}{2R}+\frac{1}{R^3}\right]\eta d\xi d\eta - \frac{k^2}{2}I_\eta' - I_\eta'' \quad (18)$$

are the integrals over triangular domains represented as the sums of regular and singular parts, and the singular integrals

$$I_0' = \int_{\eta=0}^{1}\int_{\xi=0}^{1-\eta}\frac{1}{R}d\xi d\eta \quad (19)$$

$$I_\xi' = \int_{\eta=0}^{1}\int_{\xi=0}^{1-\eta}\frac{\xi d\xi d\eta}{R} \quad (20)$$

$$I'_\eta = \int_{\eta=0}^{1} \int_{\xi=0}^{1-\eta} \frac{\eta d\xi d\eta}{R} \tag{21}$$

and

$$I''_0 = \int_{\eta=0}^{1} \int_{\xi=0}^{1-\eta} \frac{1}{R^3} d\xi d\eta \tag{22}$$

$$I''_\xi = \int_{\eta=0}^{1} \int_{\xi=0}^{1-\eta} \frac{1}{R^3} \xi d\xi d\eta \tag{23}$$

$$I''_\eta = \int_{\eta=0}^{1} \int_{\xi=0}^{1-\eta} \frac{1}{R^3} \eta d\xi d\eta \tag{24}$$

are the so-called potential integrals, since they don't depend on the frequency of excitation.

The first terms of (13)–(18) are regular and may be easily evaluated using Gaussian procedure specially developed for the triangular domains [19]. The singular integrals (19)–(21), arisen in calculating impedance matrix elements, are well studied in MoM literature [20, 21] and found to give finite values at any observation points including those on the triangle plane. This is the case also for calculating the vector potential (10). Another case occurs with integrals (22)–(24), arisen in field computations since, although they were studied in literature [21], but are essentially singular (tend to infinity), when the observation point approaches to the triangle plane. This problem can however be overcome, when analyzing the complete expressions for partial potentials (11), (12), and utilizing the original evaluation of potential integrals (22)–(24) presented in [15].

Let us analyze, for the reasons of brevity, only essentially singular parts of integrals (22)–(24) to be of the form [15]

$$I_0''^{\,sing} = I''_0 = \frac{1}{2A_n^\pm} \frac{\alpha'}{d} \tag{25}$$

$$I_\xi''^{\,sing} = \frac{-(2BC - ED)I''_0}{4AB - E^2} \tag{26}$$

$$I_\eta''^{\,sing} = \frac{-(2AD - EC)I''_0}{4AB - E^2} \tag{27}$$

where d is the distance from the observation point to the plane of triangle, α' is the parameter defined by the triangle geometry [15], and

$$A = |\vec{r}_2 - \vec{r}_1|^2, \quad B = |\vec{r}_3 - \vec{r}_1|^2, \quad C = -2(\vec{r} - \vec{r}_1) \cdot (\vec{r}_2 - \vec{r}_1)^2$$
$$D = -2(\vec{r} - \vec{r}_1) \cdot (\vec{r}_3 - \vec{r}_1), \quad E = 2(\vec{r}_2 - \vec{r}_1) \cdot (\vec{r}_3 - \vec{r}_1), \quad F = |\vec{r} - \vec{r}_1|^2$$

Substituting designations above into (26) and (27) and making use of vector identities [18]

$$(\vec{a} \times \vec{b}) \cdot (\vec{c} \times \vec{d}) = (\vec{a} \cdot \vec{c})(\vec{b} \cdot \vec{d}) - (\vec{a} \cdot \vec{d})(\vec{b} \cdot \vec{c})$$

we transform (26) and (27) to

$$I_\xi''^{\,sing} = \frac{(\vec{r}_3 - \vec{r}_1) \cdot \{[(\vec{r}_2 - \vec{r}_1) \times (\vec{r}_3 - \vec{r}_1)] \times (\vec{r} - \vec{r}_1)\}}{[(\vec{r}_2 - \vec{r}_1) \times (\vec{r}_3 - \vec{r}_1)]^2} I_0'' \tag{26a}$$

$$I_\eta''^{\,sing} = -\frac{(\vec{r}_2 - \vec{r}_1) \cdot \{[(\vec{r}_2 - \vec{r}_1) \times (\vec{r}_3 - \vec{r}_1)] \times (\vec{r} - \vec{r}_1)\}}{[(\vec{r}_2 - \vec{r}_1) \times (\vec{r}_3 - \vec{r}_1)]^2} I_0'' \tag{27a}$$

Further, we substitute (25), (26a) and (27a) into (11) and (12) and introduce the unit normal vector to the triangle plane

$$\hat{n} = \frac{(\vec{r}_2 - \vec{r}_1) \times (\vec{r}_3 - \vec{r}_1)}{|(\vec{r}_2 - \vec{r}_1) \times (\vec{r}_3 - \vec{r}_1)|}$$

to obtain the following expressions for the singular parts of the potentials sought

$$\vec{\nabla}\Phi_n^{\pm sing} = \pm \frac{\ell_n}{i2\pi\omega\varepsilon} \frac{\alpha'}{2A_n^\pm} \hat{n}^\pm \tag{28}$$

$$\vec{\nabla} \times \vec{A}_n^{\pm sing} = \mp \frac{\mu \ell_n}{4\pi} \frac{\alpha'}{2A_n^\pm} \hat{n}^\pm \times (\vec{r} - \vec{r}_n^{\,\pm}) \tag{29}$$

where $\hat{n}^\pm = \hat{n}$, when observation point lies from the direction of positive normal to the triangle plane, and $\hat{n}^\pm = -\hat{n}$ otherwise.

Formulas (28) and (29) give bounded values for the essentially singular parts of potentials (11) and (12) being continues when approaching the triangle plane, but discontinuous, when passing this plane. These discontinuities however have the physical origin and are caused by the charges and currents on the surface of triangle.

Hence, formulas (10)–(12), together with (13)–(29) and details of [15], completely describe the fields scattered by the triangulated geometries at any observation points including those on the triangle plane. Note, that these formulas are general enough, when using basis functions (8), and may be utilized both for conventional single-point testing procedure [14], and for ε-Rao and enhanced (including Galerkin) integration technique [22].

3. RESULTS

BCP error metric (3a) was applied to examine convergence and estimate accuracy of MoM solutions for a number of geometries using triangle doublet basis functions and single-point Galerkin testing procedure for EFIE [14]. All the calculations were performed by original Tri-Dimensional code "TriD" [15].

First, the scattering problem on open cube geometry of the size $\lambda \times \lambda \times \lambda$ was analyzed when exposed to the normally incident plane wave, polarized along its horizontal side (Fig. 1).

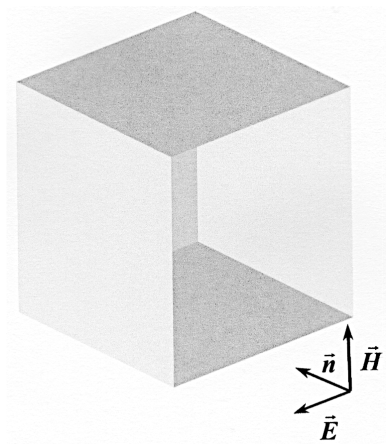

Figure 1. Problem geometry.

Fig. 2 shows the BCP errors of the obtained solutions versus the number n of triangles per the side of uniformly triangulated open cube. For comparison, two integration scheme results are presented here: 1-point scheme utilizing field values in the centers of triangles, and, more accurate, 9-point scheme [21] applying Gaussian integration over the surface of triangles. These results indicate that BCP error is monotonically decreased with increasing the number of triangles. Besides, BCP errors calculated by 9-point scheme are essentially greater than those obtained by 1-point scheme. This means that the applied testing procedure imposes boundary conditions being more favorable for the centers of triangles.

Figs. 3(a,b) show the correlation of BCP errors with errors of near-field characterization of the problem for the current and charge distributions, respectively. The charge distribution error was evaluated using an error metric similar to (1). As a benchmark solution, solution for the sufficiently fine cube geometry with $n = 60$ ($N = 54120$

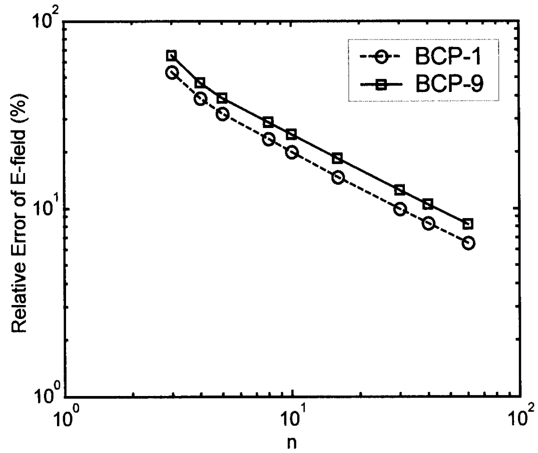

Figure 2. Relative BCP error of electric field for two integration schemes versus the number of triangles per the side of the open cube.

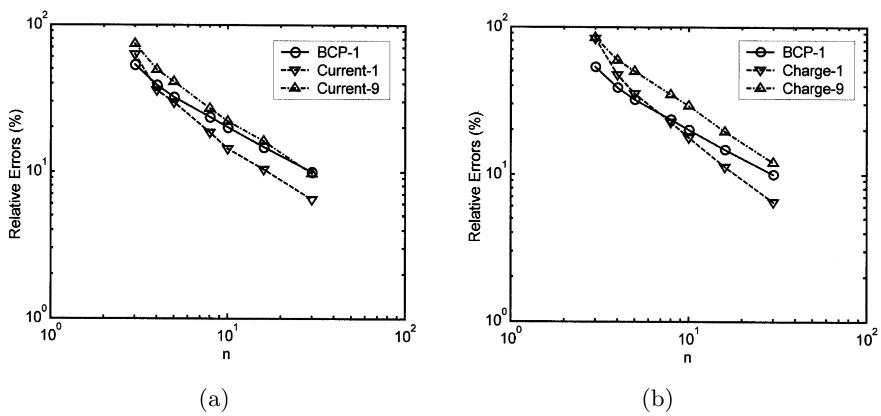

Figure 3. Comparison of 1-point relative BCP error with current (a) and charge (b) distribution errors.

unknowns) was utilized. For approximation purposes, currents and charges in the centers of triangles with BCP error of 6% were applied. These results reveal that BCP error for electric field is closely related with those for current and charge distributions. Moreover, starting from the certain n, this error lies between the 1-point and 9-point current and charge distribution errors.

To examine the contributions of separate geometry elements to

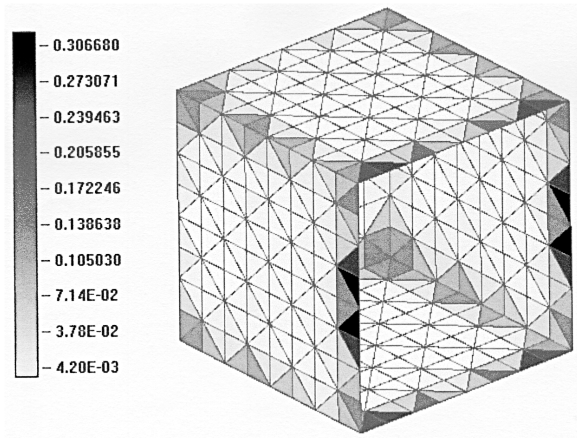

(a)

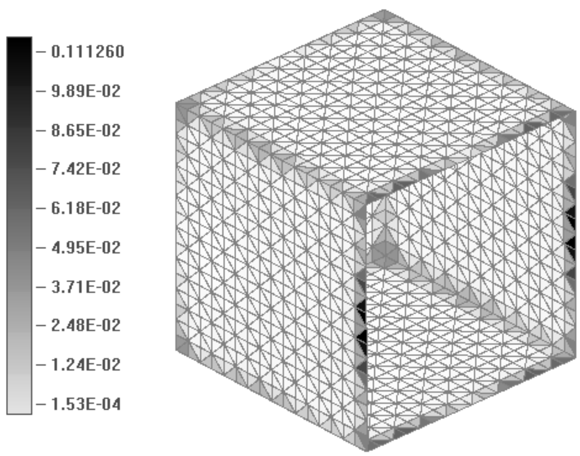

(b)

Figure 4. Distribution of partial BCP errors on open cube geometry calculated by 9-point integration scheme for $n = 8$ (a) and $n = 16$ (b).

the total BCP error, Figs. 4(a, b) show the distributions of partial BCP errors on the surface of triangulated cube calculated by 9-point integration scheme for the coarse ($n = 8$) and refined ($n = 16$) geometries, respectively. The values of partial errors on separate triangles are shown on color bars presented at the left. These distributions show, that maximum contributions to the total BCP error are associated with geometry elements distributed along the open

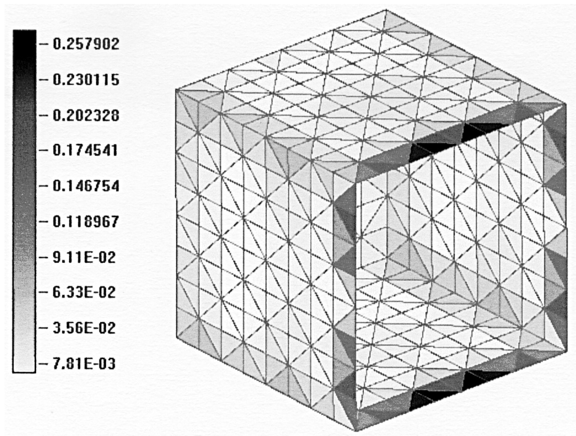

(a)

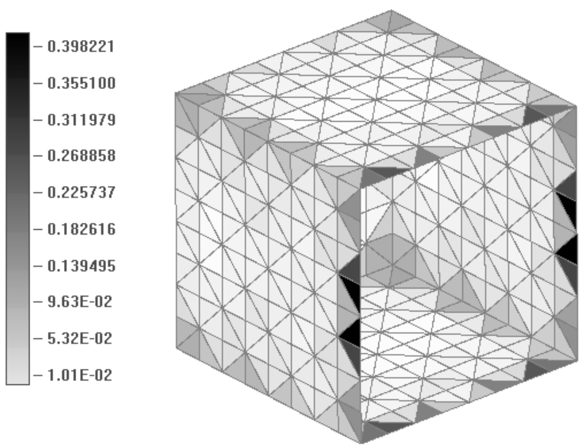

(b)

Figure 5. Distribution of current (a) and charge (b) partial errors on open cube geometry calculated by 9-point integration scheme for $n = 8$.

sides of the cube. Besides, the significant contributions to the total error are also produced by the elements distributed nearby rectangular bends between the cube facets. Finally, comparison of the results for the coarse and refined geometries reveals the significant reduction (in 3 times) of maximum partial errors with increasing the number of triangles (in 2 times per side), resulted in decreasing of the total BCP error (in 3/2 times).

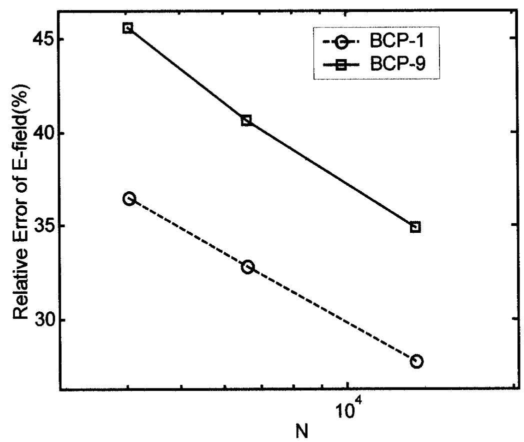

Figure 6. BCP error on triangulated car model versus the number of unknowns N calculated for 1-point and 9-point integration schemes.

To find the correlation of partial BCP errors with errors of near-field characteristics, Figs. 5(a, b) present the partial errors of current and charge distributions on open cube surface. The comparison of partial BCP errors with those for current and charge distributions reveals a good agreement between BCP and charge distribution errors. However, maximum partial BCP error lies between the maximum current and charge distribution errors.

Next, BCP error metric (3a) was applied to estimate accuracy of MoM solutions for the realistic car model excited from the top by an incident plane wave polarized along the length of the car at frequency $f = 300\,\text{MHz}$.

Fig. 6 displays the BCP errors of the obtained solutions for almost uniformly triangulated car geometries versus the number of unknowns. In this Figure, 3 cases of triangulations for the same model are presented: 2709 triangles (4028 unknowns), 4449 triangles (6602 unknowns), and 8998 triangles (13340 unknowns). It is seen, that solution error is monotonically reduced with increasing the number of unknowns (triangles). However, even for the fine mesh with 8998 triangles, BCP error is of 27.8% (for observation in the centers of triangles), and 34.9% (for 9-point integration over triangles).

Fig. 7 shows the distribution of partial BCP errors on the surface of the fine (8998 triangles) car geometry, calculated by 9-point scheme. From this Figure, it is clearly seen, that maximum partial errors (0.184% per triangle) are observed nearby the back doors of the car. The significant errors are also detected in vicinity of the free

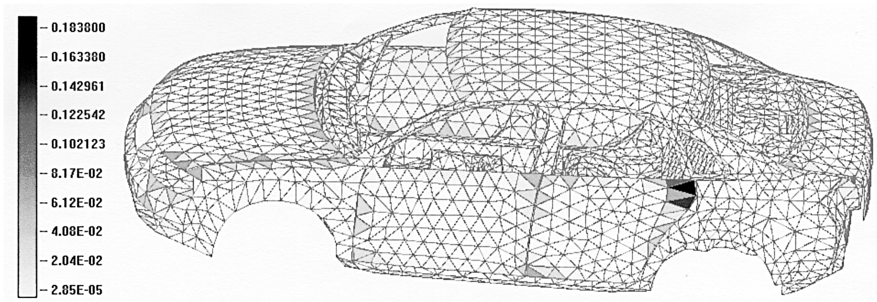

Figure 7. Distribution of partial BCP errors on triangulated car model (8998 triangles) calculated by 9-point integration scheme.

borders and slots between the car elements that requires more tidy consideration of these elements.

Thus, BCP error allows estimating accuracy of MoM solutions on purely 3-D geometries both on total structure and its separate parts.

4. DISCUSSION

The presented results show, that BCP error metric (3a) allows us to properly describe the solution convergence for arbitrary 3-D geometries, to give the reasonable values of the total error correlated with those for near-field characteristics, and to find the contributions of separate geometry elements to the total error on the boundary surface.

In particular, from Fig. 2 it follows, that uniformly increasing the number of triangles, one can attain any desired accuracy of the solution. Fig. 3 shows, that BCP error is directly correlated with errors of near-field electromagnetic characterization of the problem. Fig. 4 reveals the mechanism of accumulation of the total error, allowing us to find the geometry elements the worst contributed to the total error. Fig. 5 shows the correlation of partial BCP errors with those for near-field characteristics. And finally, Figs. 6 and 7 applies the BCP error metric for realistic car model geometry to find out both the quality of the mesh used and the recommendations for its refinement.

From the analysis above it follows, that BCP error metric allows evaluating accuracy of MoM solutions in near-field region on any surface configurations, including those with free boundaries. The values of the obtained errors reflect the maximum errors of near-field characteristics, which are decreased when moving from the boundary surface. In the same time, this error metric has an advantage over other near-field error metrics since it needs not a refined geometry or benchmark solution for its estimation.

Finally, BCP error metric may be applied to compare various triangulations for the same model, to modify the currently used basis functions and testing procedures, and to create a new adaptive MoM scheme by property indicating geometry elements, which are worst contributed to the total error on the structure. These extensions will be done in our further works.

5. CONCLUSIONS

In this work, a new error metric, based on checking boundary conditions performance (BCP) on the scatterer surface, has been applied for estimating accuracy of MoM solutions on purely 3-D geometries for triangle doublet basis functions. For this purpose, accurate expressions for the scattered field have been derived to be valid at any observation points including those on the surface of triangles. Further, the BCP error metric has been applied to the scattering problem solution on open cube geometry. A close correlation of BCP error with those for the current and charge distributions has been revealed based on rather accurate solution for the sufficiently fine cube geometry (54120 unknowns). Next, the BCP error metric has been applied to estimate accuracy of MoM solutions on the realistic car geometry. Finally, possibilities of the BCP error metric for further developments have been outlined.

REFERENCES

1. Harrington, R. F., *Field Computation by Moment Methods*, IEEE Press, New York, 1993.
2. Tekin, I. and E. H. Newman, "Method of moment solution for a wire attached to an arbitrary faceted surface," *IEEE Trans. Antennas & Propagat.*, Vol. AP 46, 559–562, 1998.
3. Nakano, H. and K. Nakayama, "A curved spiral antenna above a conducting cylinder," *IEEE Trans. Antennas & Propagat.*, Vol. AP-47, 3–8, 1999.
4. Taboada, J. M., J. L. Rodrigues, and F. Obelleiro, "Comparison of moment-method solutions for wire antennas attached to arbitrarily shaped bodies," *Microwave & Opt. Techn. Letters*, Vol. 26, 413–419, 2000.
5. Neumayer, R., A. Stelzer, F. Haslinger, G. Steinmair, M. Troscber, J. Held, B. Unger, and R. Weigel, "Numerical EMC simulation

for automotive applications," *IEEE Antennas Propagat. Mag.*, Vol. 45, 29–38, 2003.

6. Duffy, A. P., M. S. Woolfson, and T. M. Benson, "Use of correlation functions to assist the experimental validation of numerical modelling techniques," *Microwave & Opt. Techn. Letters*, Vol. 7, 361–364, 1994.
7. Williams, A. J. M., A. P. Duffy, M. S. Woolfson, and T. M. Benson, "A powerful new technique for the quantitative validation of modelled and experimental data," *Microwave & Opt. Techn. Letters*, Vol. 17, 284–287, 1998.
8. Kolundžija, B. M., "Accurate solution of square scatterer as benchmark for validation of electromagnetic modeling of plate structures," *IEEE Trans. & Antennas Propagat.*, Vol. AP-46, 1009–1014, 1998.
9. Hsiao, G. C. and R. E. Kleinman, "Mathematical foundations for error estimation in numerical solutions of integral equations in electromagnetics," *IEEE Trans. Antennas & Propagat.*, Vol. AP-45, 316–328, 1997.
10. Miller, E. K., "PCs for AP and other EM reflections," *IEEE Antennas & Propagat. Mag.*, Vol. 42, 98–101, 2000.
11. Poggio, A. J. and E. K. Miller, "Integral equation solutions of three-dimensional scattering problems," *Computer Techniques for Electromagnetics*, R. Mittra (ed.), Pergamon, New York, 1973.
12. Amitay, N., V. Galindo, and Ch. P. Wu, *Theory and Analysis of Phased Array Antennas*, Wiley-Intersience, New York, 1972.
13. Davidson, D. B., I. P. Theron, U. Jakoblls, F. M. Landstorfer, F. J. C. Meyer, J. Mostert, and J. J. van Tonder, "Recent progress on the antenna simulation program FEKO," *Proc. of IEEE South African Symp. on Commun. and Signal Processing, COMSIG*, Capetown, 427–430, 1998.
14. Rao, S., D. Wilton, and A. Glisson, "Electromagnetic scattering by surfaces of arbitrary shape," *IEEE Trans. & Antennas Propagat.*, Vol. AP-30, 409–418, 1982.
15. Bogdanov, F. G., R. G. Jobava, and S. Frei, "About evaluation of the potential integrals for near field calculations in MoM solution to EFIE for triangulated surfaces," *Proc. of IEEE VII Intern. Seminar/Workshop DIPED-2002*, 113–117, Lviv-Tbilisi, Georgia, 2002.
16. Van Bladel, J., *Electromagnetic Fields*, McGraw-Hill, New York, 1964.
17. Zienkiewicz, O. C., *The Finite Element Method in Engineering*

Science, McGraw-Hill, New York, 1971.
18. Korn, G. A. and T. M. Korn, *Mathematical Handbook for Scientists and Engineers*, McGraw-Hill, New York, 1961.
19. Abramovitz, M. and A. I. Stegun, *Handbook of Mathematical Functions*, Dover Publications, New York, 1970.
20. Rao, S. M., A. W. Glisson, D. R. Wilton, and B. S. Vidula, "A simple numerical solution procedure for static problems involving arbitrary-shaped surfaces," *IEEE Trans. Antennas & Propagat.*, Vol. AP-27, 604–608, 1979.
21. Graglia, R. D., "On the numerical integration of the linear shape functions times the 3-D Green's function or its gradient on a plane triangle," *IEEE Trans. Antennas & Propagat.*, Vol. AP-41, 1448–1455, 1993.
22. Bücker, M., "Enhanced numerical integration technique," *IEEE 1999 International EMC Symposium*, 328–333, Seattle, Washington, 1999.

Faik G. Bogdanov was born in Tbilisi, Georgia, in 1956. He received the M.S., Ph.D. and D.S. degrees in Radiophysics from Tbilisi State University, Tbilisi, Georgia, in 1978, 1983, and 1993, respectively. From 1980 to 1983 he served as a Research Scientist in Radiophysics Department of Tbilisi State University. Since 1983 he has been with Georgian Technical University, Tbilisi, Georgia as a Senior Scientist, Associate Professor (from 1984) and Professor (from 1994). Currently he is a Head of Development Department of Electro-Magnetic Consulting and Software, group (EMCoS), Tbilisi, Georgia. His research interests include electromagnetic scattering and absorption, electrodynamics of complex media, antenna analysis and design, electromagnetic compatibility, computational electrodynamics, and software development.

Roman G. Jobava was born in Georgia, formerly USSR, in 1965. He received his Ph.D. degree in Radiophysics from Tbilisi State University, Tbilisi, Georgia, in 1990. Since 1991 he has been working at the Sukhumi Branch of Tbilisi State University and was appointed as Associate Professor in 1996. From 1987 to 2000 he was a Senior Researcher in Laboratory of Applied Electrodynamics of Tbilisi State University, responsible for computer simulation of transient electromagnetic phenomena and development of appropriate numerical and software tools. In 2001 he began leading an Electro-Magnetic Consulting and Software group (EMCoS). His research interests include numerical methods in applied electrodynamics, computer simulation of EMC problems, ESD, and transient field calculations.

Stephan Frei was born in 1966 in Hanau, Germany. He received his diploma in 1995 and his Ph.D. degree in 1999 both in Electrical Engineering from the Technical University of Berlin. From 1995 till 1999 he was a research assistant in the Institute of Electrical Power Engineering on the Technical University of Berlin. There he worked on ESD, fast pulse measurement methods, and numerical calculations. Currently he is working in the automotive industry in the EMC-department of Audi in Germany. There he is responsible for numerical methods and the computation of automotive EMC, component testing methods, ESD and standardization.